Intensity-dependent three-body Coulomb explosion of methane in femtosecond laser pulses

Chuanpeng Cao,[1] Min Li,[1,*] Keyu Guo,[1] Zichen Li,[1] Yang Liu,[1] Yupeng Liu,[1] Kunlong Liu,[1] Yueming Zhou,[1] and Peixiang Lu[1,2]

[1]*School of Physics and Wuhan National Laboratory for Optoelectronics, Huazhong University of Science and Technology, Wuhan 430074, China*

[2]*Optics Valley Laboratory, Wuhan 430074, China*

(Received 31 July 2023; accepted 19 January 2024; published 20 February 2024)

We experimentally study three-body Coulomb explosion of methane molecules, i.e., $CH_4^{3+} \rightarrow H^+ + H^+ + CH_2^+$ in 800-nm laser pulses with different intensities. We find that, at a relatively low intensity, the three-body breakup channel is dominated by a concerted pathway with a high kinetic energy release (KER). However, at a high laser intensity, an extra pathway with a low KER appears. The pathway with a low KER can be explained as a sequential pathway, indicating the potential existence of a stable intermediate CH_3^{2+} dication during the three-body Coulomb explosion of methane molecules in strong laser pulses. The intensity dependence of the pathway is explained as the increasing population on the excited state of CH_3^{2+} with the increase of the laser intensity, which has a longer lifetime than that of the ground state.

DOI: 10.1103/PhysRevA.109.023115

I. INTRODUCTION

Methane is a significant organic molecule owing to its simple structure. It is widely distributed throughout the universe and can easily become a highly charged molecular ion through ionization by cosmic radiation. Subsequently, the highly charged molecular ions can generate fragments via dissociation or Coulomb explosion (CE) processes [1–5]. Therefore, studying the fragmentation dynamics of methane molecules can aid in our understanding of atmospheric chemistry and interstellar chemistry [2–5]. Moreover, the methane molecule serves as an ideal prototype to investigate some fundamental effects, such as Jahn-Teller distortion [6,7] and Auger decay [8].

The fragmentation dynamics has been extensively studied when the methane molecules are irradiated by strong laser fields or impacted by ion or electron sources in the last few decades [9–17]. A lot of attention has been focused on the three-body breakup channels of $CH_4^{2+} \rightarrow H + H^+ + CH_2^+$ and $CH_4^{3+} \rightarrow H^+ + H^+ + CH_2^+$. The three-body fragmentation processes are usually classified into two classes, namely, concerted and sequential pathways [9–16]. In the concerted pathway, two C-H bonds break simultaneously [15,16,18,19]. In the sequential pathway, one chemical bond breaks after the other breaks with a time delay, resulting in the formation of a long-lived intermediate ion [18–28]. For the three-body fragmentation processes of $CH_4^{2+} \rightarrow H + H^+ + CH_2^+$, the experimental results with ion impact have excluded the existence of the sequential pathway of $CH_4^{2+} \rightarrow H + CH_3^{2+} \rightarrow H + H^+ + CH_2^+$ [10,16]. A similar conclusion was obtained in electron impact experiments [11,12,15]. In the laser-induced CE process of the methane molecules, it was found that the three-body channel of $CH_4^{3+} \rightarrow H^+ + H^+ + CH_2^+$ occurs in a concerted process while the sequential pathway involving a long-lived intermediate CH_3^{2+} dication was not observed [13]. These results all indicate the absence of a long-lived CH_3^{2+} dication, which is consistent with a previous theoretical study that the ground state CH_3^{2+} dication should not have a significant lifetime. This is because the ground state potential energy curve has a local well too shallow to support a long-lived state [29].

In fact, long-lived dications are important for determining double ionization energy value and studying bond-forming reactions [3,30]. There were many attempts to directly observe the long-lived CH_3^{2+} dication [30–34]. In the 1980s, some groups claimed to directly observe the long-lived CH_3^{2+} dication using the charge stripping technique [30,31]. However, subsequent experiments using the same method did not find the long-lived CH_3^{2+} dication [32–34]. Furthermore, when methane was irradiated by femtosecond laser fields [35,36] or impacted by electrons and ions [10,12,15,16], the CH_3^{2+} dication was not observed in time-of-flight spectra. While the existence of long-lived CH_3^{2+} dications remains controversial, most of the experimental results support the theoretical study, i.e., the CH_3^{2+} dication usually has a short lifetime [29]. However, those previous studies only considered the ground state of the CH_3^{2+} dication. In strong laser fields, it has been shown that the population of the excited state increases with increasing the laser intensity [37,38].

In this paper, we investigate the dependence of the three-body fragmentation process of CH_4^{3+} on the intensity of a strong 800-nm laser pulse. Our primary focus is the breakup channel of $CH_4^{3+} \rightarrow H^+ + H^+ + CH_2^+$. We find that a pathway with a high kinetic energy release (KER) (high-KER pathway) is dominant in the three-body CE process of CH_4^{3+} at a relatively low laser intensity. However, when increasing the laser intensity, an additional pathway with a low KER (low-KER pathway) is observed. The low-KER pathway can

*mli@hust.edu.cn

be explained as a sequential pathway. One possible explanation would be the existence of a stable intermediate CH_3^{2+} dication. Furthermore, we have calculated the ground and excited state potential energy curves for the CH_3^{2+} dication. The ground state potential energy curve exhibits a shallow potential well, while the potential energy curve of the electronic excited state reveals a deep potential well. This indicates that the excited state CH_3^{2+} dication should have a long lifetime. Moreover, using the concerted pathway, we also reconstruct the transient molecular structure of CH_4^{3+} at the instant of CE. These results underscore the importance of laser parameters in the three-body fragmentation of methane molecules, offering new avenues for controlling the outcome of methane molecule fragmentation reactions under strong laser fields.

II. EXPERIMENTAL METHODS

The CE experiment of methane molecules in intense laser fields was conducted using cold-target recoil-ion momentum spectroscopy (COLTRIMS). A Ti:sapphire laser system produced linearly polarized laser fields with a central wavelength of 800 nm and a pulse width of ∼25 fs. The laser intensity was regulated by an 800-nm half-wave plate and an ultrabroadband wire grid polarizer made of fused silica. Subsequently, the laser beam was focused into the vacuum chamber by a parabolic mirror ($f = 75$ mm) and interacted with the supersonic methane molecules. Three-dimensional momentum distributions of the ions were measured via the COLTRIMS. A weak homogeneous static electric field (∼10.2 V/cm) was utilized to accelerate and guide the resultant ions to microchannel plate detectors. By measuring the time of flight and the positions of the ions on the detectors, three-dimensional photoion momentum distributions with high resolution can be obtained. We obtained the results of the CE channel of $CH_4^{3+} \rightarrow H^+ + H^+ + CH_2^+$ at two laser intensities. The intensity was calibrated by comparing the photoelectron momentum distribution from single ionization of argon in elliptically polarized laser pulses with the result of the nonadiabatic tunneling ionization model [39]. The laser intensity of the lower intensity case was calibrated to be around 1.8×10^{14} W/cm^2, while that of the higher intensity case was calibrated to be around 3.8×10^{14} W/cm^2.

III. RESULTS AND DISCUSSION

The total KER distributions (blue solid lines with squares) for the channel of $CH_4^{3+} \rightarrow H^+ + H^+ + CH_2^+$ at different laser intensities are shown in Fig. 1. At the laser intensity of 1.8×10^{14} W/cm^2, the KER distribution exhibits only one peak at ∼15.5 eV in Fig. 1(a), which corresponds to the high-KER pathway. However, at the laser intensity of 3.8×10^{14} W/cm^2, an additional peak at ∼8.8 eV appears alongside the peak ∼15.5 eV in the KER spectrum of Fig. 1(b), which corresponds to the low-KER pathway.

To shed light on the origin of the high-KER pathway and the low-KER pathway, we utilize the ion kinetic energy (KE) correlation spectrum to analyze the three-body fragmentation dynamics [19,24]. We show the ion KE correlation spectrum of two protons in Figs. 2(a) and 2(b) at the laser intensity of 1.8×10^{14} W/cm^2 and 3.8×10^{14} W/cm^2, respectively. In

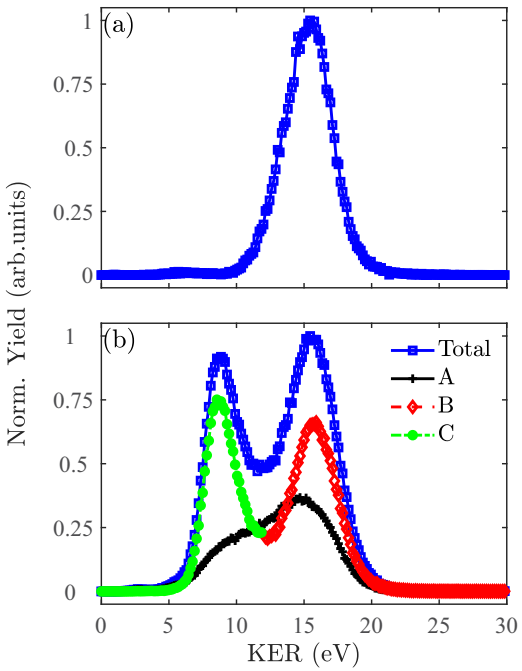

FIG. 1. The blue solid lines with squares show the total ionic KER distributions for the three-body breakup channel $CH_4^{3+} \rightarrow H^+ + H^+ + CH_2^+$ at the laser intensity of (a) 1.8×10^{14} W/cm^2 and (b) 3.8×10^{14} W/cm^2. The black solid line with plus signs shows the KER distribution of region A in Fig. 2(b). The red dashed line with rhombuses shows the KER distribution of region B in Fig. 2(b). The green dash-dotted line with circles shows the KER distribution of region C in Fig. 2(b).

Fig. 2(a), the ion KE correlation spectrum mainly lies near the diagonal line of the coordinate axis at the low laser intensity, marked as region A. Additionally, a winglike structure marked as region B in Fig. 2(a) is observed, but the proportion of the events in region B is relatively small. When increasing the laser intensity, the ion KE correlation spectrum in

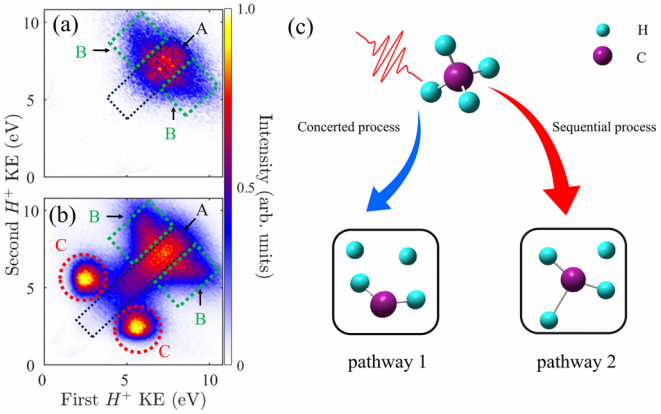

FIG. 2. (a) and (b) The ion KE correlation spectrum for two protons generated from the CE channel $CH_4^{3+} \rightarrow H^+ + H^+ + CH_2^+$ at the laser intensity of 1.8×10^{14} W/cm^2 (a) and 3.8×10^{14} W/cm^2 (b). (c) The schematic diagram for the concerted pathway (pathway 1) and the sequential pathway (pathway 2) for the three-body CE process of CH_4^{3+}.

Fig. 2(b) becomes complex. Regions A and B are also found in Fig. 2(b), but the proportion of the events in region B of Fig. 2(b) obviously increases as compared to that in Fig. 2(a). Moreover, an interesting observation in Fig. 2(b) is that two isolated islands marked as region C appear, which exhibit an obvious asymmetric energy sharing between the two protons. Furthermore, the KER distributions of regions A–C are shown in Fig. 1(b). It is noted that regions A and B mainly contribute to the peak of ∼15.5 eV in the KER spectrum, i.e., the high-KER pathway. Region C corresponds to the peak of ∼8.8 eV, i.e., the low-KER pathway. According to previous studies [19,40], regions A–C should originate from different fragmentation processes.

For the three-body channel of $CH_4^{3+} \rightarrow H^+ + H^+ + CH_2^+$, the concerted and sequential pathways are illustrated in Fig. 2(c), namely,

$$\text{pathway 1:}\quad CH_4^{3+} \rightarrow H^+ + H^+ + CH_2^+$$

$$\text{pathway 2:}\quad CH_4^{3+} \rightarrow H^+ + CH_3^{2+} \rightarrow H^+ + H^+ + CH_2^+.$$

In the case of pathway 1, two C-H bonds break simultaneously. When those two C-H bonds stretch symmetrically and break simultaneously, the two protons acquire the same KEs at the moment of breakup and thus the KE correlation spectrum shows a distribution along the diagonal line of the coordinate axis. This corresponds to the concerted pathway with symmetric stretching. When the two C-H bonds break with different bond lengths at the moment of breakup in pathway 1, the two protons acquire different KEs, which corresponds to the concerted pathway with asymmetric stretching. In the case of pathway 2, there is a delay between the breaking of two C-H bonds and it will also produce two protons with asymmetric energy sharing. Based on the above analysis, region A of the high-KER pathway in Fig. 2 should correspond to the concerted pathway with symmetric stretching. Regions B and C both exhibit a pronounced asymmetric energy distribution between the two protons. In order to provide a more comprehensive illustration of the fragmentation mechanisms occurring in different regions as depicted in Figs. 2(a) and 2(b), we show Dalitz plots in Fig. 3 and Newton plots in Fig. 4. Here, we only show the results at high laser intensity in Figs. 3 and 4.

The Dalitz plots presented in Fig. 3 can serve as a valuable visualization tool for the three-body fragmentation processes [18]. This probability density represents the vector correlation by utilizing the reduced energies of the three fragments, denoted as X and Y according to the equations

$$X = \frac{\epsilon_1 - \epsilon_2}{\sqrt{3}}$$

$$Y = \epsilon_3 - \frac{1}{3}. \tag{1}$$

Here, $\epsilon_i = |\mathbf{P_i}|^2 / \sum |\mathbf{P_j}|^2$ $(i, j = 1, 2, 3)$ represents the normalized coordinate of the ith fragment and $\mathbf{P_i}$ represents the momentum vector of the ith fragment. In our analysis, the two protons are regarded as the first and second fragments, and CH_2^+ is regarded as the third fragment. The Dalitz plots corresponding to regions A–C of Fig. 2(b) are shown in Figs. 3(a), 3(b), and 3(c), respectively. Note that the Dalitz plots at the case of lower laser intensity are nearly the same as those in Figs. 3(a) and 3(b). Additionally, Fig. 3(d) displays the characteristic momentum vector geometries for specific points in the Dalitz plot. Moreover, the Newton plot in Fig. 4 is also an effective method to identify the fragmentation mechanisms of three-body processes. For the Newton plots in Fig. 4, the normalized momenta of the three fragments are plotted on a two-dimensional plane with one of them fixed on the x axis and the other two on the upper and lower half planes. The Newton plots corresponding to regions A, B, and C of Fig. 2(b) are displayed in Figs. 4(a), 4(b), and 4(c), respectively.

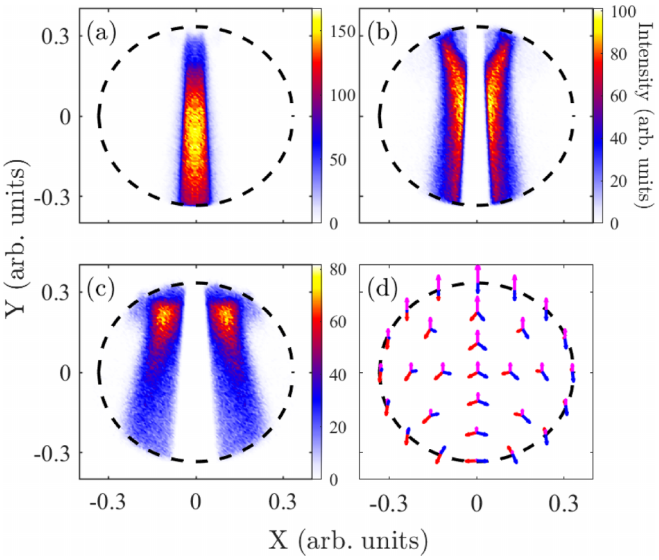

FIG. 3. (a)–(c) Dalitz plots for the three-body fragmentation of CH_4^{3+} at the laser intensity of 3.8×10^{14} W/cm^2, corresponding to regions A–C in Fig. 2(b). (d) Characteristic momentum vector geometries for specific points in the Dalitz plot.

For region A, the Dalitz plot in Fig. 3(a) is primarily distributed along $X = 0$. The results, by comparing Fig. 3(a) with Fig. 3(d), indicate that the two protons acquire the same energy during the three-body fragmentation process. The corresponding Newton plot in Fig. 4(a) shows a pair of crescent-shaped structures. These results support that region A in Fig. 2(b) arises from the concerted pathway with symmetric stretching.

For region B, the Dalitz plot and the Newton plot are shown in Figs. 3(b) and 4(b), respectively. Notably, the events

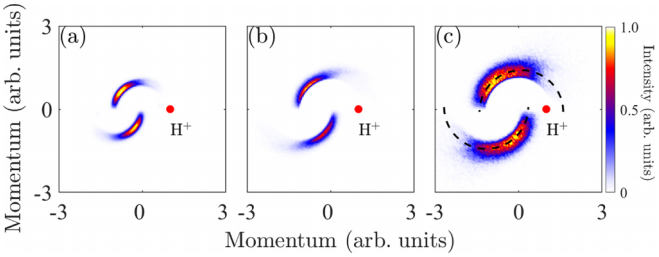

FIG. 4. (a)–(c) Newton plots for the three-body fragmentation of CH_4^{3+} at the laser intensity of 3.8×10^{14} W/cm^2, corresponding to -regions A–C in Fig. 2(b). The black dashed line in Fig. 4(c) is meant to guide the eye.

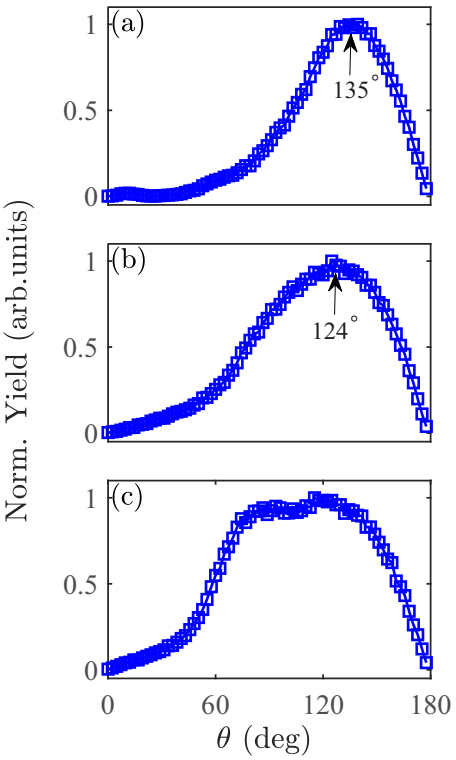

FIG. 5. The correlation angle distributions between the momentum vectors of two protons for regions A (a), B (b), and C (c) in Fig. 2(b), respectively.

in region B are close to those in region A on the Dalitz plot. It is found that as the KE of one proton decreases, the KE of the other proton increases for region B of Fig. 2. This shows a strong asymmetric KE correlation, which is consistent with the expected behavior of two asymmetrically stretching C-H bonds. The result is also consistent with previous results [40]. For the Newton plot in Fig. 4(b), it also exhibits a pair of crescent-shaped structures, which is similar to the result for the concerted pathway with symmetric stretching. As for region C, the Dalitz plot and the Newton plot are shown in Figs. 3(c) and 4(c). Notably, the events in region C are significantly distant from those in region A on the Dalitz plot. This indicates that the three-body fragmentation mechanisms for regions A and C should be different. Although the Newton plot in Fig. 4(c) is more like an incomplete semicircular structure, the differences of the Newton plot between region B and region C are not obvious enough. Therefore, we further show the correlation angle distribution between the momentum vectors of the two protons in Fig. 5.

Figure 5(a) shows the correlation angle distribution between the momentum vectors of the two protons in region A of Fig. 2(b). The distribution exhibits a single-peak structure at 135°, indicating the presence of the most probable relative emission direction between the two protons when the two C-H bonds break. Similarly, the correlation angle distribution between the momentum vectors of the two protons in region B, shown in Fig. 5(b), also exhibits a single-peak structure at 124°. However, in Fig. 5(c), it can be seen that the angular distribution exhibits a plateau-like distribution

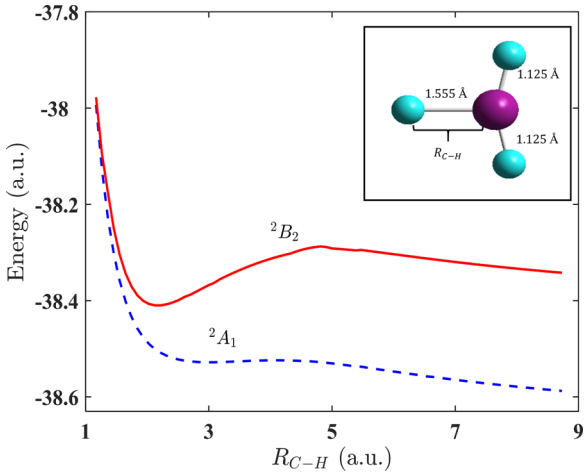

FIG. 6. Potential energy curves of CH_3^{2+}. The blue dashed line is the potential energy curve of the ground state ($^2A_1$ state). The red solid line is the potential energy curve of the excited state ($^2B_2$ state). The inset shows the equilibrium geometrical structure of the CH_3^{2+}.

within an angle range of 80°–140°, which is different from the single-peak structures in regions A and B. This indicates a lack of correlation in the emission angles of the two protons, which agrees with the expected behavior of the sequential pathway. Therefore, region B is more likely to originate from the concerted pathway with asymmetric stretching, closely associated with the vibrational motion of the chemical bond. Region C is more likely to originate from the sequential process, closely related to the rotation of the intermediate.

From the above analysis, it is found that the concerted pathway is dominant for the three-body CE channel of $CH_4^{3+} \rightarrow H^+ + H^+ + CH_2^+$ at low laser intensity. This is consistent with previous studies, i.e., the absence of the long-lived CH_3^{2+} dication [16,29]. However, when increasing the laser intensity, it is found that the low-KER pathway may originate from the sequential pathway $CH_4^{3+} \rightarrow H^+ + CH_3^{2+} \rightarrow H^+ + H^+ + CH_2^+$. One possible explanation for this result is the existence of a stable CH_3^{2+} dication, which is different from previous theoretical study [29].

We employed the CASSCF/CASPT2/cc-pVQZ method to calculate potential energy curves of the CH_3^{2+} dication in the quantum chemistry software of ORCA [41–43]. The selected active space comprises five electrons and seven orbitals, and we also verified the selected active space using the MOKIT package [44]. Firstly, we optimized a structure of the CH_3^{2+} dication, which is depicted in the inset of Fig. 6. The geometry exhibits a C_{2v} symmetry and reveals a long C-H bond, which corresponds to a weak one-electron bond [29]. Subsequently, we varied the C-H bond length of this weak bond while keeping other bond angles and lengths fixed to obtain the potential energy curves. The corresponding results are shown in Fig. 6. The ground state of CH_3^{2+} dication corresponds to the $^2A_1$ state, whose potential energy curve is shown by the blue dashed line in Fig. 6. It is evident that the potential energy curve of the ground state CH_3^{2+} dication exhibits a negligible potential well and resembles a repulsive potential curve. According to previous studies, the lifetime of the

dications is related to the depth of the potential well on the potential energy curve [16,27,29,35]. Therefore, this implies that the ground state CH_3^{2+} dication should not have a significant lifetime, which agrees with previous studies [29,35] and cannot explain our experimental results at high laser intensity.

We further investigated the potential energy curve of the $^2B_2$ state CH_3^{2+} dication, as shown by the red solid line in Fig. 6. It is found that the potential energy curve of the $^2B_2$ state exhibits a deep potential well. Therefore, the result indicates that a stable excited state CH_3^{2+} dication is feasible and potentially has a long lifetime. The long-lived intermediate dications rotate during the CE process, which leads to a lack of correlation in the emission angles of the two protons. Therefore, the correlation angle distribution between the two protons shows a plateau-like structure, as shown in Fig. 5(c). Moreover, in Fig. 1(b), the KER value of region C is lower compared to that of regions A and B. Previous studies have shown that excited states typically yield higher KER values in the three-body breakup channels as compared to the ground state by assuming the final dissociation limit is identical for the ground and excited states (the dissociation limit refers to the energy of potential energy curve when the bond length goes to infinity) [28,40]. However, in our case, the final dissociation limit of the $^2B_2$ state is much higher than that of the $^2A_1$ state, as shown in Fig. 6, which leads to a lower KER value of region C than that of regions A and B in Fig. 1(b). Furthermore, when increasing the laser intensity, the population on the excited state of CH_3^{2+} also increases [38] and the low-KER pathway appears.

Our experimental and theoretical results indicate that the most likely reason for the low-KER pathway is the presence of long-lived CH_3^{2+} dication, leading to the sequential pathway. However, the complex nuclear dynamics in the potential energy surface during multiple ionization poses challenges in fully comprehending the experimental results, presented in Figs. 4 and 5. In order to provide a more direct evidence for the existence of long-lived CH_3^{2+} dication, *ab initio* theoretical calculation may be needed. Moreover, considering the complex vibrational modes and light mass of the hydrogen atom in methane, the influence of the large angle vibration of two C-H bonds cannot be entirely ruled out with regards to the experimental results in region C. Therefore, the experimental results do not decisively confirm the presence of the long-lived CH_3^{2+} dication. We hope that our experimental results can facilitate a detailed theoretical study about the low-KER pathway.

Moreover, the most probable molecular geometry of CH_4^{3+} is reconstructed, using the information encoded in the concerted pathway with symmetric stretching. To reconstruct the molecular geometry at the instant of CE, we employ the classical Coulomb model [22,24]. The molecular geometry of neutral CH_4 and the reconstructed molecular geometry of CH_4^{3+} are both depicted in Fig. 7(a). As can be seen, the two C-H bonds stretch to ∼4.7 a.u. and the bond angle is approximately 113° at the instant of CE. We further rule out the possible non-Coulomb effect during our reconstruction process [19]. To this end, we calculated the *ab initio* potential energy curve of CH_4^{3+} using the CASSCF method with the quantum chemistry software ORCA, assuming equal

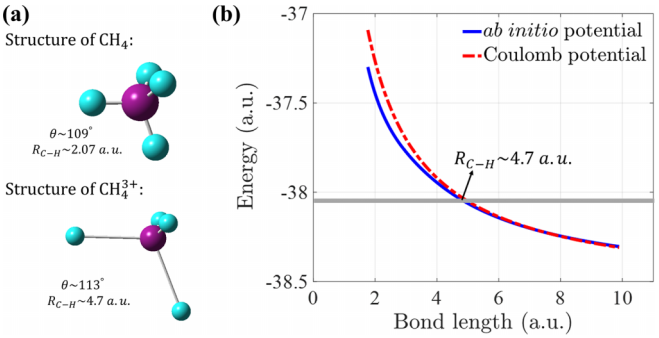

FIG. 7. (a) The molecular geometric structure of neutral CH_4 and the reconstructed molecular geometric structure of CH_4^{3+} using the concerted pathway with symmetric stretching. (b) The Coulomb potential and *ab initio* potential of CH_4^{3+}. Here, the selected two C-H bond lengths are equally stretched, while the other two C-H bonds are fixed to be 1.09 Å and the bond angles are fixed to be 109°28′.

bond lengths for the two stretching C-H bonds. The results are shown in Fig. 7(b). Remarkably, it can be observed that the *ab initio* potential energy curve agrees with the Coulomb potential energy curve when the bond length exceeds 4.7 a.u.. This indicates that the classical Coulomb model is suitable for reconstructing the molecule geometry and the non-Coulomb effect is not significant in our case [19]. The reconstructed results indicate that the most probable bond length stretches to approximately 2.3 times the equilibrium bond length of the neutral molecule, which is consistent with previous results in the CE process of some other molecules [45]. The reconstructed bond angle is nearly identical to that of the neutral molecule.

IV. CONCLUSIONS

We have investigated the intensity-dependent three-body fragmentation dynamics of CH_4^{3+} in a strong 800-nm femtosecond laser field. At low laser intensities, it is found that the dominant pathway is the high-KER pathway, which is believed to be a concerted pathway. As the laser intensity increases, a low-KER pathway emerges. Our results indicate that this pathway might originate from a sequential pathway $CH_4^{3+} \rightarrow H^+ + CH_3^{2+} \rightarrow H^+ + H^+ + CH_2^+$, which suggests the existence of a stable CH_3^{2+} dication. Our theoretical results reveal that the potential energy curve of the excited state CH_3^{2+} dications possesses a deep potential well, enabling the formation of long-lived CH_3^{2+} dications. Consequently, the population of the excited state CH_3^{2+} dications increases with increasing laser intensity and the low-KER pathway appears. Additionally, employing the CE imaging method, the structure of CH_4^{3+} at the moment of CE has been reconstructed. This comprehensive investigation enhances our understanding of the three-body fragmentation dynamics of methane molecules, suggesting an evidence for the presence of long-lived CH_3^{2+} dications during the CE processes of methane molecules. Such results may hold promise for investigations of time-resolved chemical reactions [46,47].

ACKNOWLEDGMENTS

This work was supported by the National Key Research and Development Program of China (Grant No. 2019YFA0308300) and the National Natural Science Foundation of China (Grants No. 62275085 and No. 12021004). The computation is completed in the HPC Platform of Huazhong University of Science and Technology. We are grateful to Shirong Wang from Fudan University for his assistance with the quantum chemistry calculations.

[1] V. Formisano, S. Atreya, T. Encrenaz, N. Ignatiev, and M. Giuranna, Detection of methane in the atmosphere of mars, Science **306**, 1758 (2004).

[2] A. G. G. M. Tielens, The molecular universe, Rev. Mod. Phys. **85**, 1021 (2013).

[3] R. Thissen, O. Witasse, O. Dutuit, C. S. Wedlund, G. Gronoff, and J. Lilensten, Doubly-charged ions in the planetary ionospheres: A review, Phys. Chem. Chem. Phys. **13**, 18264 (2011).

[4] E. F. van Dishoeck, Astrochemistry: Overview and challenges, Proc. Int. Astron. Union **13**, 3 (2017).

[5] D. K. Böhme, Multiply-charged ions and interstellar chemistry, Phys. Chem. Chem. Phys. **13**, 18253 (2011).

[6] M. Li, M. Zhang, O. Vendrell, Z. Guo, Q. Zhu, X. Gao, L. Cao, K. Guo, Q. Q. Su, W. Cao, S. Luo, J. Yan, Y. Zhou, Y. Liu, Z. Li, and P. Lu, Ultrafast imaging of spontaneous symmetry breaking in a photoionized molecular system, Nat. Commun. **12**, 4233 (2021).

[7] E. Ridente, D. Hait, E. A. Haugen, A. D. Ross, D. M. Neumark, M. Head-Gordon, and S. R. Leone, Femtosecond symmetry breaking and coherent relaxation of methane cations via x-ray spectroscopy, Science **380**, 713 (2023).

[8] I. B. Ortenburger and P. S. Bagus, Theoretical analysis of the Auger spectra of CH_4, Phys. Rev. A **11**, 1501 (1975).

[9] G. Dujardin, D. Winkoun, and S. Leach, Double photoionization of methane, Phys. Rev. A **31**, 3027 (1985).

[10] I. Ben-Itzhak, K. D. Carnes, S. G. Ginther, D. T. Johnson, P. J. Norris, and O. L. Weaver, Fragmentation of CH_4 caused by fast-proton impact, Phys. Rev. A **47**, 3748 (1993).

[11] R. Flammini, M. Satta, E. Fainelli, G. Alberti, F. Maracci, and L. Avaldi, The role of the methyl ion in the fragmentation of CH_4^{2+}, New J. Phys. **11**, 083006 (2009).

[12] M. D. Ward, S. J. King, and S. D. Price, Electron ionization of methane: The dissociation of the methane monocation and dication, J. Chem. Phys. **134**, 024308 (2011).

[13] J. B. Williams, C. S. Trevisan, M. S. Schöffler, T. Jahnke, I. Bocharova, H. Kim, B. Ulrich, R. Wallauer, F. Sturm, T. N. Rescigno, A. Belkacem, R. Dörner, T. Weber, C. W. McCurdy, and A. L. Landers, Imaging polyatomic molecules in three dimensions using molecular frame photoelectron angular distributions, Phys. Rev. Lett. **108**, 233002 (2012).

[14] R. Singh, P. Bhatt, N. Yadav, and R. Shanker, Ionic fragmentation of a CH_4 molecule induced by 10-keV electrons: Kinetic-energy-release distributions and dissociation mechanisms, Phys. Rev. A **87**, 062706 (2013).

[15] B. Wei, Y. Zhang, X. Wang, D. Lu, G. C. Lu, B. H. Zhang, Y. J. Tang, R. Hutton, and Y. Zou, Fragmentation mechanisms for methane induced by 55 eV, 75 eV, and 100 eV electron impact, J. Chem. Phys. **140**, 124303 (2014).

[16] Y. Zhang, T. Jiang, L. Wei, D. Luo, X. Wang, W. Yu, R. Hutton, Y. Zou, and B. Wei, Three-body fragmentation of methane dications produced by slow Ar^{8+}-ion impact, Phys. Rev. A **97**, 022703 (2018).

[17] J. Rajput, D. Garg, A. Cassimi, A. Méry, X. Fléchard, J. Rangama, S. Guillous, W. Iskandar, A. N. Agnihotri, J. Matsumoto, R. Ahuja, and C. P. Safvan, Unexplained dissociation pathways of two-body fragmentation of methane dication, J. Chem. Phys. **156**, 054301 (2022).

[18] N. Neumann, D. Hant, L. P. H. Schmidt, J. Titze, T. Jahnke, A. Czasch, M. S. Schöffler, K. Kreidi, O. Jagutzki, H. Schmidt-Böcking, and R. Dörner, Fragmentation dynamics of CO_2^{3+} investigated by multiple electron capture in collisions with slow highly charged ions, Phys. Rev. Lett. **104**, 103201 (2010).

[19] C. Wu, C. Wu, D. Song, H. Su, Y. Yang, Z. Wu, X. Liu, H. Liu, M. Li, Y. Deng, Y. Liu, L. Peng, H. Jiang, and Q. Gong, Nonsequential and sequential fragmentation of CO_2^{3+} in intense laser fields, Phys. Rev. Lett. **110**, 103601 (2013).

[20] X. Ding, M. Haertelt, S. Schlauderer, M. S. Schuurman, A. Y. Naumov, D. M. Villeneuve, A. R. W. McKellar, P. B. Corkum, and A. Staudte, Ultrafast dissociation of metastable CO^{2+} in a dimer, Phys. Rev. Lett. **118**, 153001 (2017).

[21] J. Rajput, T. Severt, B. Berry, B. Jochim, P. Feizollah, B. Kaderiya, M. Zohrabi, U. Ablikim, F. Ziaee, K. P. Raju, D. Rolles, A. Rudenko, K. D. Carnes, B. D. Esry, and I. Ben-Itzhak, Native frames: Disentangling sequential from concerted three-body fragmentation, Phys. Rev. Lett. **120**, 103001 (2018).

[22] H. Yuan, S. Xu, E. Wang, J. Xu, Y. Gao, X. Zhu, D. Guo, B. Ma, D. Zhao, S. Zhang, S. Yan, R. Zhang, Y. Gao, Z. Xu, and X. Ma, Fragmentation dynamics of a carbon dioxide dication produced by ion impact, J. Phys. Chem. Lett. **13**, 7594 (2022).

[23] T. Severt, Z. L. Streeter, W. Iskandar, K. A. Larsen, A. Gatton, D. Trabert, B. Jochim, B. Griffin, E. G. Champenois, M. M. Brister, D. Reedy, D. Call, R. Strom, A. L. Landers, R. Dörner, J. B. Williams, D. S. Slaughter, R. R. Lucchese, T. Weber, C. W. McCurdy, *et al.*, Step-by-step state-selective tracking of fragmentation dynamics of water dications by momentum imaging, Nat. Commun. **13**, 5146 (2022).

[24] K. Lin, X. Hu, S. Pan, F. Chen, Q. Ji, W. Zhang, H. Li, J. Qiang, F. Sun, X. Gong, H. Li, P. Lu, J. Wang, Y. Wu, and J. Wu, Femtosecond resolving photodissociation dynamics of the SO_2 molecule, J. Phys. Chem. Lett. **11**, 3129 (2020).

[25] X. Hu, Y. Peng, X. Zhu, S. Yan, L. Liu, W. Feng, D. Guo, Y. Gao, S. Zhang, D. Zhao, D. Dong, B. Hai, J. Xu, S. Zhang, X. Ma, J. Wang, and Y. Wu, Breakdown of the Coulomb-explosion imaging technique induced by the ultrafast rotation of fragments, Phys. Rev. A **101**, 012707 (2020).

[26] X. Yu, X. Zhang, X. Hu, X. Zhao, D. Ren, X. Li, P. Ma, C. Wang, Y. Wu, S. Luo, and D. Ding, Femtosecond time-resolved neighbor roles in the fragmentation dynamics of molecules in a dimer, Phys. Rev. Lett. **129**, 023001 (2022).

[27] X. L. Zhu, X. Q. Hu, S. C. Yan, Y. G. Peng, W. T. Feng, D. L. Guo, Y. Gao, S. F. Zhang, A. Cassimi, J. W. Xu, D. M. Zhao, D. P. Dong, B. Hai, Y. Wu, J. G. Wang, and X. Ma, Heavy N^+ ion transfer in doubly charged N_2Ar van der Waals cluster, Nat. Commun. **11**, 2987 (2020).

[28] A. Méry, X. Fléchard, S. Guillous, V. Kumar, M. Lalande, J. Rangama, W. Wolff, and A. Cassimi, Investigation of the carbon monoxide dication lifetime using $(CO)_2$ dimer fragmentation, Phys. Rev. A **104**, 042813 (2021).

[29] J. A. Pople, B. Tidor, and P. von Ragué Schleyer, The structure and stability of dications derived from methane, Chem. Phys. Lett. **88**, 533 (1982).

[30] T. Ast, C. J. Porter, C. J. Proctor, and J. H. Beynon, Doubly charged molecular ions of methane, Chem. Phys. Lett. **78**, 439 (1981).

[31] P. G. Fournier, J. Fournier, F. Salama, P. J. Richardson, and J. H. D. Eland, Formation and dissociation of doubly ionized methane, J. Chem. Phys. **83**, 241 (1985).

[32] C. J. Proctor, C. J. Porter, T. Ast, P. D. Bolton, and J. H. Beynon, Charge stripping reactions of ions formed from methane, ammonia, water and hydrogen sulphide by protonation and by electron impact, Org. Mass Spectrom. **16**, 454 (1981).

[33] D. Mathur, C. Badrinathan, F. A. Rajgara, and U. T. Raheja, Translational energy loss spectrometry of molecular dications from methane, Chem. Phys. **103**, 447 (1986).

[34] Y. Levy, A. Bar-David, I. Ben-Itzhak, I. Gertner, and B. Rosner, Formation of long-lived CD_n^{2+} and CH_n^{2+} dications, J. Phys. B: At. Mol. Opt. Phys. **32**, 3973 (1999).

[35] Z. Wu, C. Wu, Q. Liang, S. Wang, M. Liu, Y. Deng, and Q. Gong, Fragmentation dynamics of methane by few-cycle femtosecond laser pulses, J. Chem. Phys. **126**, 074311 (2007).

[36] J. Strohaber, F. Zhu, A. A. Kolomenskii, and H. A. Schuessler, Observation of anisotropic fragmentation in methane subjected to femtosecond radiation, Phys. Rev. A **89**, 023430 (2014).

[37] H. Akagi, T. Otobe, A. Staudte, A. Shiner, F. Turner, R. Dörner, D. M. Villeneuve, and P. B. Corkum, Laser tunnel ionization from multiple orbitals in HCl, Science **325**, 1364 (2009).

[38] X. Xie, S. Roither, M. Schöffler, E. Lötstedt, D. Kartashov, L. Zhang, G. G. Paulus, A. Iwasaki, A. Baltuška, K. Yamanouchi, and M. Kitzler, Electronic predetermination of ethylene fragmentation dynamics, Phys. Rev. X **4**, 021005 (2014).

[39] M. Li, M. M. Liu, J. W. Geng, M. Han, X. Sun, Y. Shao, Y. Deng, C. Wu, L. Y. Peng, Q. Gong, and Y. Liu, Experimental verification of the nonadiabatic effect in strong-field ionization with elliptical polarization, Phys. Rev. A **95**, 053425 (2017).

[40] S. Xu, X. L. Zhu, W. T. Feng, D. L. Guo, Q. Zhao, S. Yan, P. Zhang, D. M. Zhao, Y. Gao, S. F. Zhang, J. Yang, and X. Ma, Dynamics of $C_2H_2^{3+} \rightarrow H^+ + H^+ + C_2^+$ investigated by 50-keV/u Ne^{8+} impact, Phys. Rev. A **97**, 062701 (2018).

[41] F. Neese, The ORCA program system, WIREs Comput. Mol. Sci. **2**, 73 (2012).

[42] F. Neese, F. Wennmohs, U. Becker, and C. Riplinger, The ORCA quantum chemistry program package, J. Chem. Phys. **152**, 224108 (2020).

[43] F. Neese, Software update: The ORCA program system - Version 5.0, WIREs Comput. Mol. Sci. **12**, e1606 (2022).

[44] J. Zou, MOKIT program, https://gitlab.com/jxzou/mokit (accessed Jan 28, 2023).

[45] I. Bocharova, R. Karimi, E. F. Penka, J. Brichta, P. Lassonde, X. Fu, D. Bandrauk, I. Litvinyuk, J. Sanderson, and J. Kieffer, Charge resonance enhanced ionization of CO_2 probed by laser Coulomb explosion imaging, Phys. Rev. Lett. **107**, 063201 (2011).

[46] S. Larimian, S. Erattupuzha, E. Lötstedt, T. Szidarovszky, R. Maurer, S. Roither, M. Schöffler, D. Kartashov, A. Baltuška, K. Yamanouchi, M. Kitzler, and X. Xie, Fragmentation of long-lived hydrocarbons after strong field ionization, Phys. Rev. A **93**, 053405 (2016).

[47] R. Wallauer, M. Raths, K. Stallberg, L. Münster, D. Brandstetter, X. Yang, J. Güdde, P. Puschnig, S. Soubatch, C. Kumpf, F. C. Bocquet, F. S. Tautz, and U. Höfer, Tracing orbital images on ultrafast time scales, Science **371**, 1056 (2021).